Highly transparent flexible clay films modified with organic polymer: structural characterization and intercalation properties

Hiroyuki Tetsuka, Takeo Ebina,* Hiroshi Nanjo and Fujio Mizukami

Received 3rd April 2007, Accepted 8th June 2007
First published as an Advance Article on the web 25th June 2007
DOI: 10.1039/b705063a

We are developing transparent flexible clay films with high thermal resistance and gas barrier properties. The clay films were fabricated by casting aqueous dispersions of synthetic Na^+-saponite mixed with various loadings of water-soluble organic polymer. In this paper, the structural, optical, and physical properties of the films are reported. The structure of these films has been found to have an alignment of densely packed clay platelets interspersed with polymer chains between clay platelet edges. The parallel stacking of clay platelets is enhanced by adsorption of anionic polymer on the positively charged edges of the clay platelets so that excellent optical transparency is maintained even for high clay loading (up to 90 wt%). Also, polymer chains bounded on particle edges are tightly confined by upper and lower layers of clay platelets, rendering these films more thermally stable. The degradation temperature of the films is more than 350 °C. Differential scanning calorimetry analysis reveals that the melting point of the polymer in the clay layers is shifted towards the higher temperature range, up to 440 °C. However, the segregation of polymers towards the film surface occurs with the polymer loading, which reduces the thermal resistance of the film due to weaker interaction of adsorbed polymer on the film's surface. Consequently, films with higher clay loading (>80 wt%) provide excellent optical and physical properties, these films will be promising for a wide variety of applications such as displays or other electronic devices.

1. Introduction

In recent years, there has been significant interest in flexible materials with high thermal resistance, transparency, and gas barrier properties. They can be used in important technological applications in the emerging field of flexible electronics. The main applications are in flat panel displays, for liquid crystal displays and organic light-emitting diodes, where physical and mechanical requirements do not permit the use of conventional rigid glass substrates. Recently, thin films of polyimide, polyethylene napthalate, and other materials have been emphasized as organic materials that can replace glass substrates because of their flexibility and durability against impact. However, they present several important drawbacks, the most serious of which is their low thermal resistance, in addition to the high permeation of gas molecules. These shortcomings pose great obstacles that must be surmounted for application to displays. Therefore, highly compliant materials combining the versatility of organic thin films with the superior physical properties of glass are strongly demanded.

Nanocomposites based on hybrids of organic polymers and inorganic materials have attracted considerable interest as new structural and functional materials that might present advantages over conventional polymers. Much attention has been devoted to layered inorganic materials such as clay minerals and layered metal oxides, especially in terms of their intercalation functionalization, and exfoliation.[1–6] Among them, clay minerals are potentially well suited to the design of hybrid composites because these comprise silicate layers in which the fundamental unit is a 1 nm-thick planar structure oriented in the *c*-axis direction: their lamellar elements have high in-plane strength, stiffness, and a high aspect ratio.[7] The smectite group is well known to have unique swelling, intercalation and ion exchange properties; moreover, their structural flexibility enables them to be made into various valuable derivatives. Several reports have shown that the dispersion of nanolayers of smectites such as montmorillonite and hectorite into organic polymers enhances their thermal stability,[8–10] mechanical strength,[11] and gas barrier properties.[12,13] Clay–polymer based nanocomposites have considerable potential for use as materials for flexible substrates. Actually, only a small amount of clay (only a few percent) is dispersed in the organic polymer matrix as a modifier to improve their physical properties. A promising means to further improve the physical properties might be to form composites by adding a high volume of clay. However, it is very difficult to form high clay-volume nanocomposite films without compromising their flexibility and transparency. Few reports about such materials exist in the literature.[14,15]

Recently, we produced highly transparent flexible clay films based on the hybridization of Na^+-saponite clay and water-soluble organic polymer.[16] They possessed high optical transparency and high flexible properties, even with clay content as high as 80 wt%. In addition, the clay films provide better physical properties than those of organic substrate materials: high thermal stability, low thermal expansion coefficient, and high gas barrier properties. For those reasons,

Research Center for Compact Chemical Process, National Institute of Advanced Industrial Science and Technology (AIST), 4-2-1 Nigatake, Miyagino-ku, Sendai 983-8551 E-mail: takeo-ebina@aist.go.jp

our clay films show high potential as flexible substrate materials for use in various optoelectronic devices. Through this study, we intend to elucidate the structural characterization and describe the formation mechanism of clay films with high flexibility and optical transparency. Additionally, we specifically examine the interactions between the organic polymer and clay host, and how these interactions affect the physical properties of nanocomposite films.

2. Experimental

The clay used in this study was a synthetic Na^+-saponite (Kunimine Industries Co. Ltd.) with the chemical formula $Na_{0.33}Mg_3Al_{0.33}Si_{3.67}O_{10}(OH)_2$. Nanocomposites were prepared from a solution containing sodium polyacrylate (SPA) with average molecular weights of 22 000–70 000. The clay was dispersed in water using a high shear mixer at a total solid concentration of 1 wt% with varying polymer concentration (5–30 wt% to the whole solid). The mixture was degassed in vacuum, then further centrifuged at 5500 rpm for 20 min to minimize the structural and optical defects by removing any remaining flocculated or unexfoliated clay impurities. It was then poured onto a Teflon sheet in a mold. After heating overnight at 60 °C, nanocomposite films with a thickness of *ca.* 100 μm were detached from the Teflon sheet.

The crystal structure and phase of the films were characterized using X-ray diffraction (XRD) (MXP18; Mac Science Ltd.) with a CuK_α source under an applied voltage of 40 kV and a current of 250 mA for diffraction angles $1^\circ \leqslant 2\theta \leqslant 70^\circ$, step width 0.02, counting time 1 s. Differential thermal analysis (DTA) and thermogravimetry (TG) were carried out using a thermogravimeter (Thermoplus TG8120; Rigaku) apparatus. Differential scanning calorimetry (DSC) measurements were performed (DSC3200SA; Bruker AXS GmbH). All thermal analyses were carried out at a constant heating rate of 5 °C min^{-1} under a N_2 atmosphere. The XPS measurements were performed using a spectrometer (5601ci; Ulvac PHI) with monochromatic MgK_a radiation source (150 μm spot diameter) of 1253.6 eV. The working pressure was $<5 \times 10^{-9}$ Pa. For depth profiling, Ar^+ ions of 3 keV with a partial pressure of 1×10^{-5} Pa were used. A different area (2×2 mm^2) of the films used for surface analysis was sputtered. The sputter rate of *ca.* 6 nm min^{-1} was determined by performing an experiment using the same experimental conditions on a SiO_2 thin film sample of known thickness. In addition, TEM observations were carried out using a transmission electron microscope (JEM 2000EX; JEOL) operating at an accelerating voltage of 200 kV. The dispersion liquid was dropped directly on a copper grid supported with a collodion membrane. Specimens for cross-section analyses were cut using a microtome (Ultracut UCT; Leica). The films' surface roughness was investigated using an atomic force microscope (AFM, NanoScopeIIIa; Veeco Instruments). The microscope was operated in tapping mode using Si single crystal tips (MPP-21100; NanoScope) with force constant of 3 N m^{-1} and drive frequency of 87.9 kHz. Scan rates were varied from 0.5 to 2 Hz. The optical transmittance spectra of the films were recorded using a UV/VIS spectrophotometer (MPS-2450; Shimadzu Corp.).

3. Results and discussion

In fact, Na^+-saponite comprises an alternate stack of negatively charged layers built up by two tetrahedral sheets of Si^{4+} and Al^{3+} ions and a central octahedral sheet of Mg^{2+} ions. The layer charge is compensated by exchangeable Na^+ ions located in the interlayer space. Fig. 1(a) presents a comparison of the XRD patterns of clay films with different polymer loadings. The (001) reflection appears between 2θ = 6.8–7.4°. The corresponding d_{001} values are about 1.25–1.30, indicating no significant change of the basal spacing despite the increased polymer content. Taking into account the saponite layer thickness of *ca.* 1 nm, the remainder corresponds to a monolayer of water molecules. Because of the negative charge on the tetrahedral sheet, hydrated exchangeable cations occupy most of the surface. Therefore, anionic SPA does not intercalate into an interlayer of saponite. The mirror index of observed XRD patterns for the clay film with polymer loading of 10 wt% is shown in Fig. 1(b), which exhibits a broad (*hk*0) reflection together with a sharp (00*l*) reflection. The clay film has an oriented texture out-of-plane, but a random structure in the in-plane direction, suggesting the formation of a stacking fault. As shown in the plot of the relative intensity for the (020) reflection [Fig. 1(c)], the addition of 10 wt% polymer substantially reduces the relative intensity, which levels off at higher polymer loading. The stacking fault in clay films was found to be improved by addition of polymer beyond 10 wt%. Fig. 1(d) shows (001) rocking curves for the clay films with polymer loadings of 5 wt% and 20 wt%. The respective full widths at half maximum (FWHM) of the (001) rocking curves were *ca.* 0.31° and *ca.*

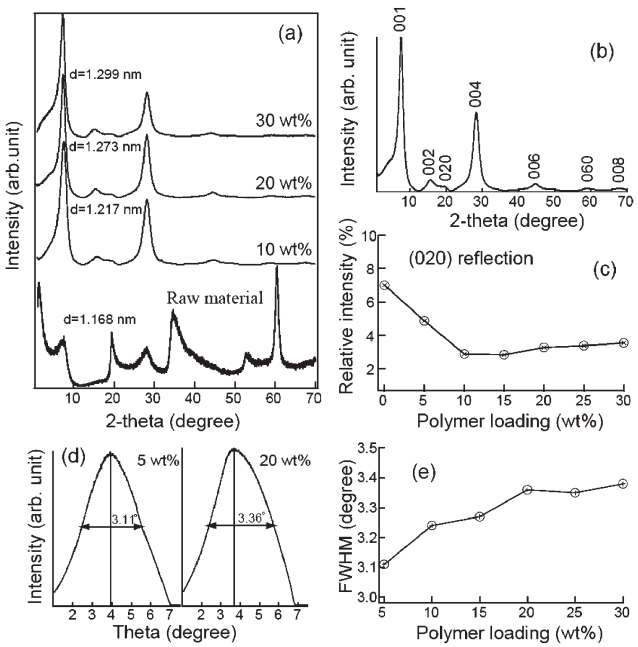

Fig. 1 Structural analyses of clay films: (a) XRD patterns from the films with different polymer loadings; (b) mirror index of the film with a polymer loading of 10 wt%; (c) relative intensity of (020) reflection *versus* (001) reflection as a function of polymer loading; (d) the (001) rocking curves corresponding to polymer loadings of 5 wt% (left) and 20 wt% (right); (e) the FWHM as a function of polymer loading.

0.36°, which suggests that the clay films had a high degree of *c*-axis preferred orientation. Fig. 1(e) shows that the FWHM increases with the increase of polymer loading, suggesting a slightly lower crystallinity.

The thermal stability of the clay films was evaluated using TG-DTA. Fig. 2(a) shows the TG-DTA curve of the clay film with a polymer loading of 20 wt%. The exothermal reaction in the DTA curve around 460 °C is caused by the decomposition of incorporated SPA molecules, which corresponds to the thermal degradation temperature of the clay films. Several stages of weight loss were apparent: (i) substantial weight loss attributable to the release of water adsorbed on the clay and the polymer (<120 °C); (ii) decomposition of the polymer (405–495 °C); and (iii) dehydroxylation of saponite around 740 °C. The DTA curves around 460 °C of the clay films with different polymer loadings are shown in Fig. 2(b). Thermal decomposition of the polymer shifted slightly toward the lower temperature range with increased polymer loading. This reduction of thermal stability might be attributed to the increase of the amount of the weakly bound polymer.

An extremely important property of our clay films is their high optical transparency. Fig. 3 illustrates the optical transmittance spectra in the visible region of the clay films with different polymer loadings. The clay films are optically highly transparent, even for clay contents as high as 90 wt%. The average transmittance of the clay films increased to a maximum value of 92% with polymer loadings up to 15 wt%; it then decreases gradually with further increased polymer loading. The transmittance of the clay film with a polymer loading of 15 wt% showed a somewhat high transmittance (90.6%) even at 350 nm. These results might originate from the reduction of the stacking faults in the clay film, as shown in the results of XRD [Fig. 1(c)]. As the stacking faults in the films decreased, light is scattered less because of the decrease in grain boundaries, which engenders higher transmittance in the visible region. However, the clay film with a polymer loading of 10 wt% indicated a lower optical transmittance than that of 15 wt% film, both have almost the same degree of stacking faults. This behaviour might be attributable to the presence of

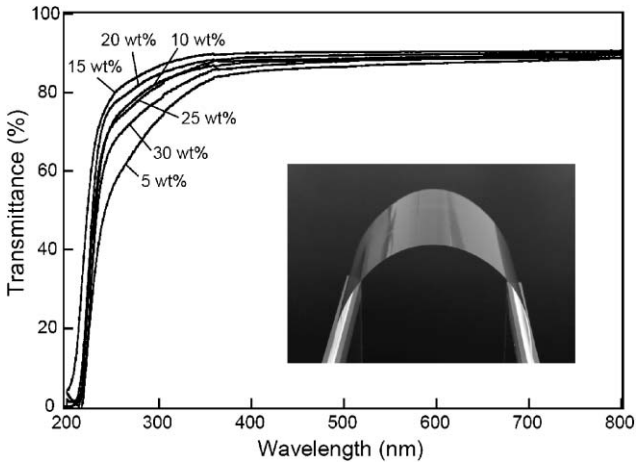

Fig. 3 Highly transparent flexible clay films. Optical transmittance spectrum in the visible region of films with different polymer loadings. The inset in the figure is a photograph of the film with a polymer loading of 20 wt%, which shows a high flexibility.

voids within the film, and is discussed in more detail in the TEM section. Composite materials are well known to suffer from increased light scattering, engendering a loss of transparency resulting from differences in the refractive indices of the materials in the composites. However, these results suggest that the refractive index of the Na^+-saponite more nearly matches that of SPA (reported to be 1.52 for saponite[17] and 1.44 for SPA). In addition, high transparency of the clay films can be maintained up to 350 °C, which is the thermal decomposition temperature of the polymer in clay. The inset in Fig. 3 shows a photograph of the clay film with a polymer loading of 20 wt%, indicating a highly flexible film. The clay film's tensile strength, as measured at a crosshead speed of 2 mm min^{-1}, achieved values near 25 MPa.

Elemental analyses and bonding characterization of the clay films were carried out using XPS. Typical XPS spectra of surfaces of the clay films with different polymer loadings are shown in Fig. 4. They have six characteristic peaks from

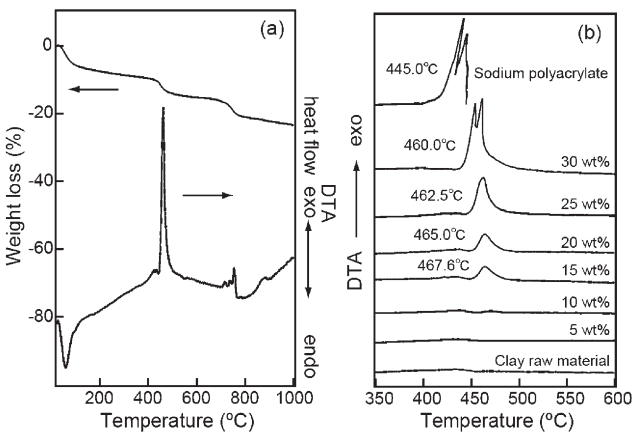

Fig. 2 Thermal analysis of clay films. (a) TG-DTA curve with the weight loss and exo-endothermal reaction of the film with a polymer loading of 20 wt%. (b) DTA curves around 460 °C of the films with different polymer loadings.

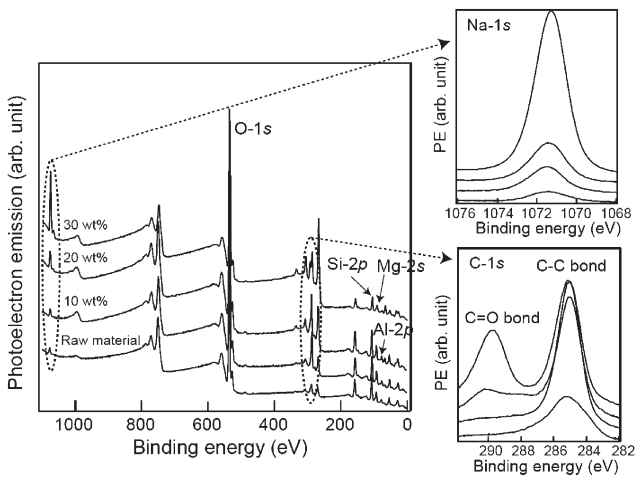

Fig. 4 XPS surface analysis of clay films with different polymer loadings. The right panels show the high-resolution spectra of the C-1s and Na-1s core level.

Table 1 Elemental composition of clay films with different polymer loadings, as obtained by XPS surface analysis

	Atomic concentration (%)					
Sample	C	O	Si	Al	Na	Mg
Raw material	12.67	55.79	16.60	4.65	1.31	8.98
5 wt%	12.07	56.04	17.05	4.52	1.38	8.95
10 wt%	19.25	50.49	15.70	4.12	1.50	8.93
15 wt%	13.91	53.03	17.10	4.40	2.56	8.99
20 wt%	14.72	53.80	15.32	4.03	3.88	8.25
25 wt%	13.68	52.84	16.42	4.05	5.04	7.97
30 wt%	17.94	50.03	9.32	2.68	14.56	5.46

carbon, oxygen, silicon, aluminum, sodium, and magnesium. The inset shows high-resolution spectra of the C-1s core level. Two different chemical states exist. The peak associated with C–C (C–H) bonding at 284.2 eV was observed for all the clay films. Another peak associated with O–C=O bonding in the carboxylic acid (COO^-) group of sodium polyacrylate $[CH_2CH(CO_2Na)]_n$ appears at a higher binding energy of 289.6 eV for the clay films with a higher polymer loading (>15 wt%). As the polymer loading increases, the O–C=O peak intensity increases. As shown in Table 1, the increase in the fraction of polymer loading decreases the clay component contents, *e.g.*, silicon, aluminum, and magnesium, in the film surface. Especially, the clay component content was revealed to be considerably smaller for the clay film with a polymer loading of 30 wt%, although addition of 30 wt% polymer greatly increased the sodium concentration. The intensity of aluminum, magnesium and silicon might be attenuated by the presence of the extra polymer layer in the surface. This predominant amount of sodium near the surface might be attributable to segregation of the polymer towards the surface of the clay films.

Fig. 5(a) and Table 2 show high-resolution XPS depth profiles of the clay film with polymer loadings of 10 wt%, which lends further insight into the nature of the clay–polymer nanocomposites. The atomic percentage of carbon in the

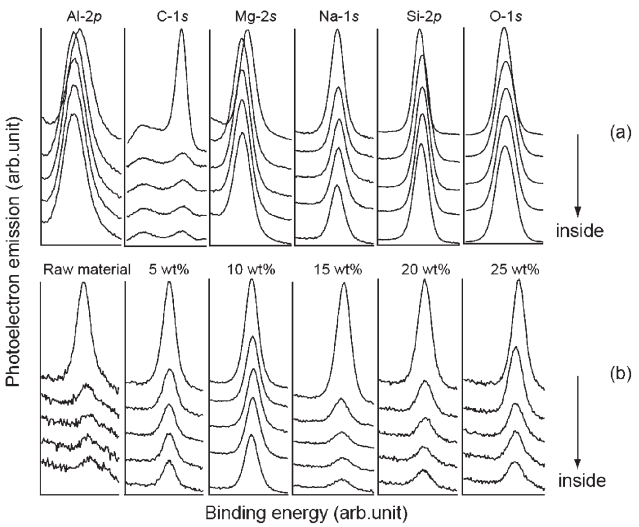

Fig. 5 XPS depth profile of clay film with a polymer loading of 10 wt% (a), the Na-1s core level from clay films with different polymer loadings (b).

Table 2 Composition of clay films as obtained by XPS depth profile

Depth (Å)	Elemental composition (%) of clay film with a polymer loading of 10 wt%					
	Si	C	O	Mg	Al	Na
0	16.06	19.96	51.86	6.61	2.86	2.65
↓	20.05	2.47	60.36	9.71	4.74	2.67
	19.32	2.22	60.23	10.68	5.06	2.49
	18.79	1.90	60.36	11.24	5.30	2.42
240	18.43	2.08	60.13	11.67	5.37	2.32

surface is much higher than that in the film interior, which is attributed to contamination by C atoms from the air. The elemental Al : Si : Mg : O molar ratio was nearly constant at 1 : 4 : 2 : 10 over the film inside for all the clay films. The sodium concentration in the film allows estimation of the amount of polymer in the film interior because the change in sodium content originates from Na^+ ions in sodium polyacrylate. The Na-1s high-resolution XPS depth profiles of the clay film with different polymer loadings are shown in Fig. 5(b) and Table 3. Results showed that the sodium content increases gradually with polymer loading up to 10 wt%, which suggests a uniform distribution of polymer into the film interior. However, for a clay film with higher polymer loading (>15 wt%), segregation of polymer occurs near the surface. It is apparent that depths to about 120 Å from the surface are enriched with sodium for films with higher polymer loading. This result must be caused by the fabrication process of the nanocomposite film. For a film with higher polymer loading, the clay precipitation occurs in the film-drying process. Therefore, the excess polymer is separated on the film surface.

The films' nanostructure was studied using TEM. Fig. 6(a) shows a TEM image in the *ab*-plane of the clay film with a polymer loading of 20 wt%. The film consists of parallel platelets of randomly arranged clay grains of *ca.* 20 nm. A model nanostructure of the clay film is presented in Fig. 6(d). The organic component seems to occupy the space between the clay particle edges; it might act as binder. The edges of the clay platelets are positively charged for the Na^+-saponite. Therefore, the anionic SPA clung to edges of the clay platelets. The flexibility of the clay films will come mainly from its unique nanostructure, which is composed of densely packed clay particles reinforced with soft organic polymer between the clay particles. Fig. 6(b) shows the selected area electron diffraction (SAED) pattern of some selected clay films. A diffraction spot disappears and shows a completely ringed pattern, which indicates lower crystallinity when the polymer loading is increased to 15 wt%. On the other hand, Fig. 7 shows a TEM image of the cross-section (*c*-axis direction) of

Table 3 Composition of clay films as obtained by XPS depth profile

Depth/Å	Sodium concentration (%) of clay film with various polymer loadings					
	Raw material	5 wt%	10 wt%	15 wt%	20 wt%	25 wt%
0	1.06	1.40	2.65	2.89	4.19	4.20
↓	0.21	1.16	2.67	0.90	1.05	1.62
	0.12	0.85	2.49	0.53	0.65	0.94
	0.12	0.74	2.42	0.45	0.42	0.73
240	0.16	0.62	2.32	0.46	0.45	0.65

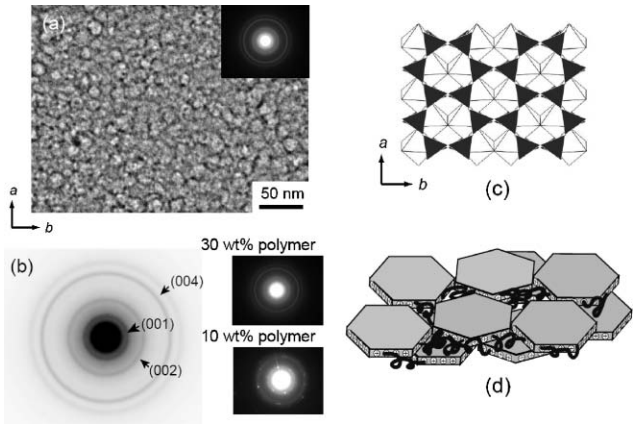

Fig. 6 TEM image and SAED patterns of clay films. (a) TEM image of the film with a polymer loading of 20 wt% on a copper grid, showing the *ab*-plane (surface) and the corresponding SAED pattern (inset). (b) SAED patterns obtained from a clay film with different polymer loadings. (c) Schematic crystal structure of saponite with [110] face. (d) Model structure of saponite–polymer nanocomposite, in which polymer occupies the space in the particle edges.

the clay film with a polymer loading of 20 wt%. The lattice fringes of the saponite (110) planes were observed in the image, which showed that all the platelets are well organized with their faces parallel to the vessel bottom. The interplanar distance is *ca.* 1.26 nm, which is consistent with the XRD results. The XRD results indicated that the addition of polymer improves the stacking of the clay platelets. Adsorption of SPA at the particle edges increases the negative edge charge density and makes the edge–face contact difficult, promoting the parallel aggregation of the layer. The stacking presents slight irregularities mainly located between layers (shown in the expanded figure), as shown in XRD analysis. Additionally, TEM images reveal that voids of *ca.* 100 nm at the maximum are present inside the film. These air spaces might give rise to light scattering because of the interfacial reflection. They are also an important factor in the decreased optical transparency of clay films. Upon impregnating the voids with polymer, however, the light scattering is reduced. The low optical transmittance of the clay film with a polymer

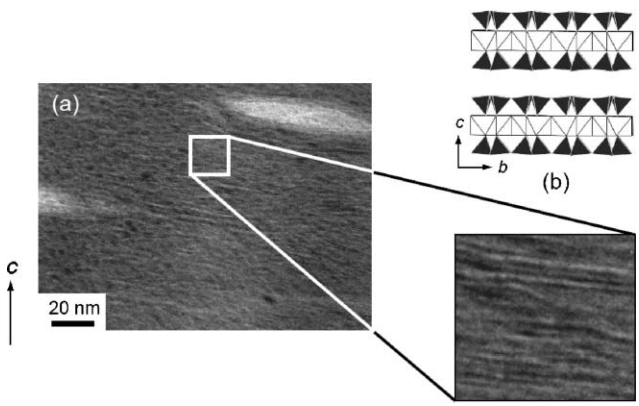

Fig. 7 TEM image of clay films. (a) TEM image of the film with a polymer loading of 20 wt%, showing the *c*-axis direction (cross-section). (b) Schematic crystal structure of saponite with [110] face.

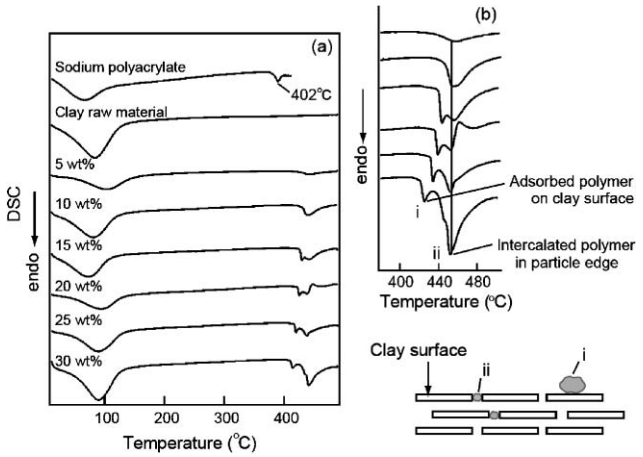

Fig. 8 Thermal analysis of clay films. (a) DSC curves of the films with different polymer loadings. Native SPA and clay raw material data are also shown for reference. (b) Expanded image of the endothermic peak around 440 °C.

loading of 10 wt% observed in Fig. 3 most likely arises from the imperfect penetration of polymer into free volume in the film.

The DSC traces for the clay films are shown in Fig. 8. Those of the clay raw material and native SPA are also shown for reference. The clay films show endothermic peaks around 90 °C and 440 °C, which might be respectively attributable to the vaporization of the water adsorbed on clay or polymer and the melting of the intercalated polymer within clay layers. Evidently, the melting point of those clay films is shifted by about 50 °C more toward the higher temperature range than native SPA, as is also implied by the TG-DTA analysis, which confirms the enhancement of thermal stability of intercalated polymer. Higher polymer loading (>15 wt%) appears to split the endothermic peak at around 440 °C. We can infer that this phenomenon reflects the structure of the clay–polymer nanocomposites. This peak's split might be the result of two competitive interactions such as those shown in the illustration of Fig. 9(b): the polymer adsorption onto the clay surface, and the intercalated polymer at the clay particle edges. The endothermic peak, which shifts toward a low temperature range with polymer loading, originates from the former polymer states, approaching that of native SPA because of the lesser interaction with clay layers. The melting point decrease indicates that the polymer in excess is indeed located at the external surfaces of the platelets. On the other hand, the latter polymer states show a strong interaction with clay platelets and therefore remain fundamentally unchanged in terms of their melting points. The polymer is fixed and stabilized among the clay platelet array by clinging onto edges of the clay particles, being sandwiched by the upper and lower layers of the clay platelets. Thus, the polymers are completely surrounded with clay platelets and fixed tightly.

The surface morphology of the clay film was investigated using AFM. Fig. 9(a) shows the topographic AFM images of the clay film with a polymer loading of 25 wt%. The AFM images show evidence of the presence of two different size particles: large spherical particles and small nanoparticles. The

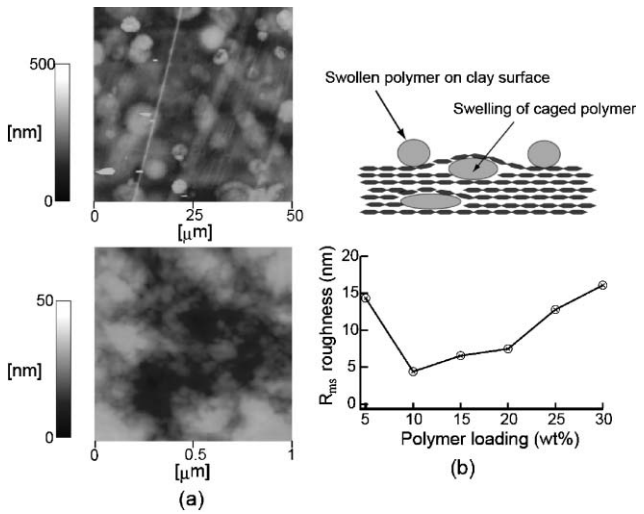

Fig. 9 AFM observations of clay film. (a) Topographic AFM images of the film surface with a polymer loading of 25 wt%. The top panel shows a large scale (scanning range 50 × 50 μm^2) image; the bottom image is of a scanning range 1 × 1 μm^2. (b) The root mean square (Rms) surface roughness as a function of polymer loading.

top image shows the presence of large spherical particles, as indicated by light and dark spots. As is illustrated schematically in Fig. 9, these large particles might correspond to an adsorbed polymer on the surface (light spots) or a caged polymer in the film interior (dark spots) that had been swollen by water adsorption. These swollen polymers might be responsible for the surface roughness. A statistical analysis of the image suggests that the heights of the spherical particles range from 200 to 300 nm and the widths range from 4 to 8 μm. For observations carried out on a smaller scale (bottom image), clay particles having diameters in the 20–40 nm range are observed. The root mean square values of surface roughness decreased with increasing polymer loading, reaching a minimum of 4.4 nm at 10 wt%, and gradually increased for higher polymer loadings [Fig. 9(b)].

4. Summary

Highly transparent flexible clay films were fabricated by casting aqueous dispersions of synthetic Na^+-saponite mixed with various loadings of sodium polyacrylate. Their high flexibility and transparency are rooted in their unique nanostructure, which comprises a dense stratified array of clay platelets with polymer chains between clay platelet edges. The anionic polymer likely acts as a soft binder connect between the clay particle edges to engender flexibility, and works to prevent the edge–face contact of clay platelets to enhance the parallel stacking of clay layers. The polymer chains bound on clay particle edges are tightly fixed by upper and lower layers of clay platelets, rendering the films more thermally stable. The melting point of polymer in the clay layers is shifted toward the higher temperature range, up to 440 °C. A uniform distribution of polymer into the film interior was achieved up to a polymer loading of 10 wt%, while the segregation of the polymer towards the film surface occurred at a higher polymer loading. The segregation of polymer into the film's surface reduces the thermal resistance of the film due to weaker interactions. Also, the swelling of the polymer by water adsorption is confirmed by AFM study, which might be responsible for the surface roughness. Consequently, the clay films with higher clay loading (>80 wt%) provide excellent optical and physical properties, these films will be promising for transparent flexible substrates for use in displays or other electronic applications.

References

1 K. Kuroda and T. Sasaki, *Science and Applications of Inorganic Nanosheets*, CMC Press, Tokyo, 2005.
2 T. J. Pinnavaia and G. W. Beall, *Polymer–Clay Nanocomposites*, John Wiley & Sons, New York, 2001.
3 R. E. Grim, *Clay Mineralogy*, McGraw-Hill, New York, 1953.
4 S. Tahara, Y. Takeda and Y. Sugahara, *Chem. Mater.*, 2005, **17**, 6198.
5 Y. Omomo, T. Sasaki, L. Wang and M. Watanabe, *J. Am. Chem. Soc.*, 2003, **125**, 3568.
6 Y. Oaki and H. Imai, *Adv. Mater.*, 2006, **18**, 1807.
7 T. J. Pinnavaia, *Science*, 1983, **220**, 365.
8 H. L. Tyan, Y. C. Liu and K. H. Wei, *Chem. Mater.*, 1999, **11**, 1942.
9 T. Lan and T. J. Pinnavaia, *Chem. Mater.*, 1994, **6**, 2216.
10 E. P. Giannelis, *Adv. Mater.*, 1996, **8**, 29.
11 Z. Wang and T. J. Pinnavaia, *Chem. Mater.*, 1998, **10**, 3769.
12 T. Lan, P. D. Kaviratna and T. J. Pinnavaia, *Chem. Mater.*, 1994, **6**, 573.
13 P. B. Messersmith and E. P. Giannelis, *Chem. Mater.*, 1994, **6**, 1719.
14 D. J. Chaiko, *Chem. Mater.*, 2003, **15**, 1105.
15 K. Haraguchi, M. Ebato and T. Takehisa, *Adv. Mater.*, 2006, **18**, 2250.
16 T. Ebina and F. Mizukami, *Adv. Mater.*, 2007, DOI: 10.1002/adma.200700162.
17 C. Klein, *The 22nd Edition of the Manual of Mineral Science*, John Wiley & Sons, Inc., New York, 2001.

